

RSC Advances



This is an *Accepted Manuscript*, which has been through the Royal Society of Chemistry peer review process and has been accepted for publication.

Accepted Manuscripts are published online shortly after acceptance, before technical editing, formatting and proof reading. Using this free service, authors can make their results available to the community, in citable form, before we publish the edited article. This *Accepted Manuscript* will be replaced by the edited, formatted and paginated article as soon as this is available.

You can find more information about *Accepted Manuscripts* in the [Information for Authors](#).

Please note that technical editing may introduce minor changes to the text and/or graphics, which may alter content. The journal's standard [Terms & Conditions](#) and the [Ethical guidelines](#) still apply. In no event shall the Royal Society of Chemistry be held responsible for any errors or omissions in this *Accepted Manuscript* or any consequences arising from the use of any information it contains.

ARTICLE

Carbon Nanotube-Polyaniline Core-Shell Nanostructured Hydrogel for Electrochemical Energy Storage

Cite this: DOI: 10.1039/x0xx00000x

Received 00th January 2012,
Accepted 00th January 2012

DOI: 10.1039/x0xx00000x

www.rsc.org/

Po-Yen Chen,^{a,b} Noémie-Manuelle Dorval Courchesne,^{a,b} Md Nasim Hyder,^{a,b} Jifa Qi,^{b,c} Angela M. Belcher,^{b,c,d,*} Paula T. Hammond^{a,b,*}

Conductive polymer hydrogels, which synergize the advantageous features of hydrogels and conductive materials, have been utilized in many electrochemical energy storage applications. Here, we introduce phytic acid as (1) a dispersing agent for pristine multi-walled carbon nanotubes (MWNTs) in aqueous solution containing aniline and as (2) a gelator to form polyaniline (PANI)-based hydrogels after polymerization. The PANI-based hydrogels exhibit nanowire-based mesoporous networks with high surface area and electrical conductivity. The nanostructured core (MWNT)-shell (PANI) hydrogels show an improvement on the electrical conductivity from 0.21 to 1.54 S cm⁻¹ as the loading of MWNTs increases from 0 to 5.0 wt.%. The conducting nanowire-based networks with MWNT loadings of 3.0 wt.% in the hydrogel provide efficient electron transport pathways that exhibit a maximal specific capacity of 609 F g⁻¹. The scalable and facile synthesis demonstrates excellent electrochemical performance, rendering it attractive for sensing, energy conversion, and energy storage applications.

Keywords: polyaniline nanowire, multi-walled carbon nanotube, conductive hydrogel, electrochemical energy storage

Introduction

Conductive polymers have received tremendous interest due to their widespread applications from energy storage devices to bioelectronics and medical applications.¹⁻⁵ Hydrogels of polyaniline (PANI), one of the most interesting electroactive polymers, receive significant attention due to facile processability, environmental stability, high electrical conductivity and redox behavior.⁶⁻⁹ To further improve the electrochemical properties (*i.e.*, electrical and ionic conductivities) of PANI-based nanostructures, incorporating carbon nanomaterials has been demonstrated as a promising approach.¹⁰⁻¹² Among various carbon nanomaterials, pristine multi-walled carbon nanotubes (MWNTs) have long been considered as ideal components for electrochemical energy storage devices due to their high electrical conductivity and aspect ratio.^{13,14}

Incorporating pristine MWNTs into PANI-based hydrogels is often challenged by the formation of non-homogeneous suspensions, and has a propensity to lead to aggregation of both the PANI nanostructures and MWNTs, resulting in the nanocomposites displaying undesired physicochemical properties. While MWNTs have been incorporated in PANI-based dried thin films using various assembly techniques, including colloidal mixture,¹⁵ interfacial polymerization,¹⁶ electrostatic deposition,^{13,14} electropolymerization,¹⁷ direct polymerization on MWNT supports,¹⁸ and enzymatic synthesis,¹⁹ these approaches cannot be applied adequately to incorporate MWNTs into hydrated PANI gels.

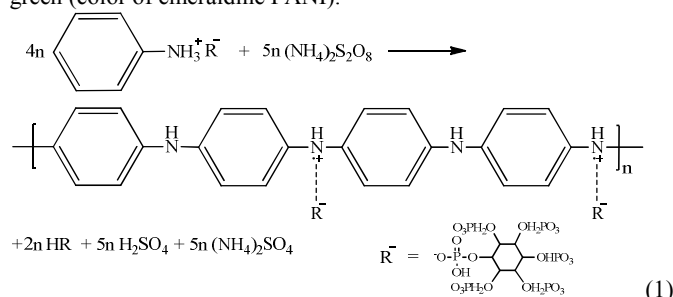
In addition, even though the MWNT aggregation in conductive hydrogels might be addressed by chemical modification of MWNTs, or by adding binders, these methods often lead to further deterioration of the electronic properties or non-uniform distribution of these materials in the nanocomposites. Therefore, an efficient approach is highly desirable to incorporate pristine MWNTs into the PANI-based hydrogels homogeneously.

Phytic acid, an abundant natural product in plant tissues, is an excellent solvent to dissolve aniline and to disperse pristine carbon nanotubes in aqueous solution homogeneously.^{20,21} Recently, phytic acid has also been used as a gelator by Boa's group due to its excellent hydrogen bonding ability for conjugated polymers.³ Herein, we have synergistically utilized the solvation and gelation properties of phytic acid to design conductive hydrogels with core (MWNT)-shell (PANI) nanostructures. After the phytic acid solution dissolves aniline and disperses MWNT homogeneously, the oxidative initiator is introduced into the mixed solution and the emeraldine PANI is then polymerized and coated on the wall surface of MWNTs to form high aspect ratio MWNT-PANI nanostructures. Also, the incorporated phytic acid serves as a dopant for as-synthesized PANI and forms hydrogen bonding between MWNT-PANI nanostructures to achieve conductive hydrogels. The resulting binder-free nanowire (NW)-based mesoporous MWNT-PANI networks provide high surface area and directional pathways for efficient electron transport. Compared to the hydrogels of PANI-

only, the MWNT-PANI nanocomposites show an improvement on the electrical conductivity from 0.21 to 1.54 S cm⁻¹ as the loading of MWNTs increases from 0 to 5.0 wt.%. In addition, the phytic acid-mediated polymerization allows efficient utilization and dispersion of pristine MWNTs within PANI nanostructures to improve the specific capacity from 460 to 609 F g⁻¹ with a low loading of pristine MWNTs (less than 3.0 wt.%). The assembly of MWNT-PANI conductive polymer hydrogels promises the fabrication of three-dimensional (3D) conducting nanocomposites with great potential in sensing, energy conversion, and energy storage applications.

Results and discussion

The fabrication process for the MWNT-PANI conductive polymer hydrogels is schematically illustrated in **Figure 1A**. First, aniline is dissolved in a 50 wt.% aqueous solution of phytic acid and then sonicated for an hour. After the mixture of aniline and phytic acid is formed, a given amount of pristine MWNTs (diameter ~ 15 nm, transmission electron microscopy (TEM) image in **Figure 1B**) is added, homogenized, ultrasonicated, and centrifuged to achieve a well-dispersed solution containing MWNTs, aniline, and phytic acid. The phytic acid-mediated approach greatly improves the dispersion of pristine MWNTs in aqueous solution (illustration shown in **Figure 1C**).^{20, 21} Phytic acid acts as a capping agent to inhibit MWNT aggregation by binding to aromatic carbon rings on the surface of pristine MWNTs via secondary interactions, and by providing a highly hydrated interface through the bound water molecules associated with its six phosphorous acid groups. After the oxidative initiator (*i.e.*, (NH₄)₂S₂O₈) is added to the phytic acid solution containing MWNTs and aniline, the polymerization of PANI (described in **Equation 1**) is indicated by a solution color change from dark brown (color of phytic acid and MWNTs) to dark green (color of emeraldine PANI).^{22, 23}



After the polymerization, each phytate moiety can interact with multiple PANI chains by doping the lone pair nitrogen of the polymer (**Figure 1A**), and by creating a hydrogen bond with neighboring phytic acid molecule thus resulting in the formation of a mesh-like hydrated fibrous network (**Figure 1D**). While the hydrogen bonding allows for the gel to maintain its stability, the doping of PANI creates electron hopping along the backbone of the PANI nanofibers to impart electronic conductivity.

The formation of PANI was confirmed by Fourier transform infrared (FTIR) measurements (**Figure 2A**); the spectrum of the MWNT-PANI hydrogel has three peaks at 1310 cm⁻¹, 1490 cm⁻¹ and 1585 cm⁻¹, which are attributed to C-N stretching, C=C stretching in the benzenoid ring, and C=C stretching in the quinoid ring, respectively.^{3, 10} Furthermore, the nitrogen and phosphorous peaks in the X-ray photoelectron spectrometer (XPS) survey scan, shown in **Figure 2B**, indicate the presence of PANI in the emeraldine state doped by phytic acid. In addition, the different carbon bonds composing the PANI backbone can be identified in the XPS C1s scan (**Figure 2C**). These include C-N, C-C, and =CH- moieties originated from the backbone of PANI. Carbon-oxygen groups and other carbon chemistries at higher binding energies belong to the phytic acid. The X-ray diffraction (XRD) patterns of PANI-only and

MWNT-PANI thin films are shown in **Figure 2D** to distinguish the solid-state crystalline structure. The XRD patterns of PANI-only and MWNT-PANI samples both show three distinct peaks at $2\theta = 15^\circ$, 22° , and 26° . The peaks in XRD patterns indicate that there is some degrees of molecular arrangement in the polymer chain, which can enhance the electronic conductivity depend on the level of doping. The peak at 22° is due to the periodicity of the polymer chains where the PANI chains are parallel to each other, and the peak at 26° is attributed to the periodicity of the polymer chains, where the chains are arranged in a perpendicular manner. It is also worth noting that the XRD pattern of MWNT-PANI sample reveals the presence of two peaks around 26° (overlapped with the peak from PANI) and 43° corresponding to the interlayer spacing of the nanotube (d_{002}) and the d_{100} reflection of the carbon atoms, respectively. The nearly identical XRD patterns between the PANI and MWNT-PANI indicate that the crystalline structures of PANI coating in both samples are similar.

The morphology of thin films are examined by scanning electron microscope (SEM), and the images are shown in **Figure 3A** and **3B**, respectively. **Figure 3A** and **Figure S1A-S1C** demonstrate that the PANI-only hydrogels generate a uniform mesoporous network composed of interconnected PANI NWs, and the average dimensions of the PANI-only NWs are 100-200 nm in diameter and 500-700 nm in length. During the polymerization process of MWNT-PANI hydrogels, 1D MWNT walls act as nucleation sites for the growth of the PANI chains, which contribute to the facile synthesis of core-shell nanostructures of MWNT and PANI. Compared to PANI-only hydrogels, the MWNT-PANI hydrogels exhibit more interconnected networks composed of NWs with higher aspect ratio (**Figure 3B**, 100-200 nm in diameter and 2-3 μm in length).

To investigate the specific surface area and pore size distribution of the PANI-based films, Brunauer-Emmett-Teller (BET) surface area analysis and Barrett-Joyner-Halenda (BJH) pore size distribution analysis were conducted on both PANI-only and MWNT-PANI samples, and the corresponding results are shown in **Figure 3C** and **3D**, respectively. From nitrogen adsorption/desorption isotherms shown in **Figure 3C**, it can be observed that the quantity of nitrogen adsorbed onto the surface of PANI and MWNT-PANI thin films is similar. The measured BET specific surface areas of PANI-only and MWNT-PANI samples are 35.1 m² g⁻¹ and 39.7 m² g⁻¹, respectively. **Figure 3D** shows the pore size distribution plots calculated using the BJH equation from the desorption branch of the isotherms. The MWNT-PANI network exhibits similar distribution curves with slightly higher pore volume than the PANI-only sample. The nitrogen adsorption/desorption isotherms and pore size distribution measurements indicate that both PANI-only and MWNT-PANI samples have porous structures mainly composed of mesopores with an average pore diameter of around 80 nm. With interconnected mesopores, the liquid electrolyte can penetrate into the structure and maximize interfacial contact with the electrolyte, thereby increasing the mobility of redox couples and minimizing back-recombination. In addition, the porosities (**Figure S2A** and **S2B**) of PANI-only and MWNT-PANI thin films are estimated by analyzing SEM images (**Figure 3A** and **3B**) with *ImageJ* software. The overall porosities of PANI-only and MWNT-PANI thin films are 36.1% and 41.7%, respectively. With 10% larger specific surface area and smaller porosity in MWNT-PANI networks, the MWNT-PANI hydrogel provides more active sites that can interact with the electrolyte, leading to higher electrochemical activities. These porous and interconnected NW-based networks with well-developed mesopores (**Figure 3D**) persist across the entire film (thickness >20 μm) and provide directional pathways for efficient electron transport throughout the porous electrode (**Figure**

3E). Such mesoporous architectures with interconnected pores maximize the interfacial contact with the electrolyte, thereby increasing the mobility of the redox couples and minimizing electron recombination.

The presence of MWNTs is confirmed by Raman spectroscopy (Figure 4A); the D-band peaks at $\sim 1350\text{ cm}^{-1}$ and G-band peaks at $\sim 1600\text{ cm}^{-1}$ from MWNTs are observed in the MWNT-PANI hydrogels. To further investigate the inner structure of the MWNT-PANI nanocomposites, the MWNT-PANI NW-based complexes were examined under SEM, and Figure 4B clearly shows that MWNTs are being utilized as scaffolds to enable the templated polymerization of PANI to form core (MWNT)-shell (PANI) nanostructures. In addition, the MWNT-PANI nanostructures are observed via TEM (shown in Figure 4C and 4D) and demonstrate that pristine MWNTs are embedded inside PANI NWs without severe aggregation of the MWNTs. The well-dispersed and embedded MWNTs are thus able to maximize the contact area with PANI coating.

The incorporation of highly conductive MWNTs enhances the electrical conductivity of thin films, and the improvement correlates strongly with the loading of MWNTs in the nanocomposites (Figure 5A). A remarkable improvement on the electrical conductivity from 0.21 to 1.54 S cm^{-1} was observed as the loading of MWNTs was increased from 0 to $5.0\text{ wt.}\%$. It is noted that when the loading of MWNTs goes above $5.0\text{ wt.}\%$, the doctor-bladed thin films begin to form large aggregates, and their surface becomes rougher, and the variation in conductivity increases (Figure S3). Therefore, the loading of MWNTs is not increased beyond $5.0\text{ wt.}\%$, and here, the MWNT-PANI composite film with a $3.0\text{ wt.}\%$ loading of MWNTs is chosen as a reference film that displays high conductivity, smooth surface, and uniform morphology.

To evaluate the electrochemical behavior of both PANI-only and MWNT-PANI hydrogels, cyclic voltammetry (CV) measurements are performed in the potential range of -0.2 V to 0.8 V (vs. Ag/AgCl reference electrode) in $1.0\text{ M H}_2\text{SO}_4$ electrolyte with Pt mesh as the counter electrode. In Figure S4A and S4B, both PANI-only and MWNT-PANI hydrogels remain stable for a wide range of scan rates from 5 to 100 mV s^{-1} . In Figure 5B, three characteristic pairs of redox peaks are evident for all of the PANI-based films, and are labeled as A/A' , B/B' and C/C' . The A/A' and C/C' peaks are associated with the redox behavior of PANI as it is cycled through the leucoemeraldine and pernigraniline states; the weak B/B' peaks are attributed to the double electron redox transition between the benzoquinone and hydroquinone through the protonation/deprotonation of PANI.¹⁵ The MWNT-PANI thin film (loading $\sim 3.0\text{ wt.}\%$) exhibits higher current density than PANI alone (scan rate 10 mV s^{-1}). Furthermore, the galvanostatic charging and discharging behaviors of both thin films are measured from 0 to 0.8 V at a discharging current of 0.1 mA cm^{-2} in a $1.0\text{ M H}_2\text{SO}_4$ electrolyte (shown in Figure 5C). The specific capacitance value, C_S (F g^{-1}), of the nanocomposites is estimated from the discharging data according to Equation 2 and the results are presented in the inset of Figure 5C.

$$C_S = I \times \Delta t / (m \times \Delta V) \quad (2)$$

where I is the charge-discharge current (A), m is the mass of the active materials (g), and $\Delta V/\Delta t$ is the rate of change (V s^{-1}) in the discharging potential obtained from the discharge trace. The highest measured C_S is $\sim 460\text{ F g}^{-1}$ for the PANI-only thin film, and $\sim 609\text{ F g}^{-1}$ for the MWNT-PANI composite film with a loading of MWNTs around $3.0\text{ wt.}\%$. The higher specific capacitance in MWNT-PANI nanocomposites originates from two charge storage mechanisms: (1) the electric double layer charge (EDLC) storage in MWNTs, and (2) the surface redox-chemistry (pseudocapacitance) of the PANI nanowires.^{13, 14, 25, 26} The improvement on the electrochemical

performance originates from the highly percolative electron conduction pathway and increased contact surface area between the well-dispersed MWNTs and coated PANI matrix. The cycle stability from the charge-discharge behavior was determined, and is presented in Figure 5D for a current rate 3.0 mA cm^{-2} for over 1500 cycles. Both of the PANI-only and MWNT-PANI electrodes exhibit a cycling stability of over 1500 cycles, with a subsequent drop ($\sim 23\%$) in specific capacitance.

Experimental

Materials. $50\text{ wt.}\%$ phytic acid aqueous solution, aniline, ammonium persulfate ($(\text{NH}_4)_2\text{S}_2\text{O}_8$), and sulfuric acid (H_2SO_4) were purchased from Sigma-Aldrich. Fluorine-dope tin oxide (FTO) glass (TEC 15, thickness = 2.2 mm) was purchased from Pilkington. Pristine multi-walled carbon nanotubes (MWNTs, outer diameter $\sim 8\text{--}15\text{ nm}$, length $\sim 10\text{--}50\text{ }\mu\text{m}$) were purchased from CheapTube. All water was deionized ($18.2\text{ M}\Omega$, mill-Q pore). All reagents were used as received and without further purification.

Generation of PANI-based hydrogels and thin films. Solution A was prepared by mixing 1.842 mL (2 mmole) $50\text{ wt.}\%$ aqueous solution of phytic acid and 0.458 mL (5 mmole) aniline. The mixed solution was sonicated for half an hour and stirred overnight. Pristine MWNTs were first mixed with solution A at a certain weight fraction, and the solution, containing phytic acid, aniline, and MWNTs, was homogenized for 1 hour and ultrasonicated for 1 hour at 40% amplitude. The resulting solution was centrifuged at 3000 r.p.m. for 10 minutes to get rid of large aggregates and to obtain well-dispersed MWNT-aniline-phytic acid solution (solution B). 0.286 g ($(\text{NH}_4)_2\text{S}_2\text{O}_8$ (1.25 mmole)) was dissolved in 1 mL milli-Q water and 1 mL $50\text{ wt.}\%$ phytic acid aqueous solution (solution C). To synthesize the PANI-only hydrogels, solution A was mixed with solution C quickly without shaking; to synthesize the MWNT-PANI hydrogels, solution B was mixed with solution C. The solutions were held at $4\text{ }^\circ\text{C}$ overnight to complete the reaction. After polymerization, the PANI-based hydrogels were dialyzed (dialysis tube, $12000\text{--}14000\text{ MW}$ cutoff) with milli-Q water and stored in room temperature. PANI-based thin films were fabricated by a doctor-blading process, and the thickness of the thin film was controlled by the tape thickness. The coated thin films were air-dried first and heated to $80\text{ }^\circ\text{C}$ to enhance the adhesion between the PANI thin film and the FTO glass.

Characterization of PANI-based thin films. Phytic acid/MWNT complex and MWNT-PANI samples were placed on transparent IR cards (International Crystal Laboratories, 19 mm KBr aperture IR card). A JASCO 4100 FTIR spectrometer was used for data collection. All spectra were obtained in absorbance mode with a resolution of 1 cm^{-1} , using 100 accumulation scans. XRD patterns were collected (PANalytical Multipurpose Diffractometer, Cu $K\alpha$ radiation operated at 45 kV and 40 mA) using a step size of 0.02° with 6.0° per minute scan speeds under the following settings: 1° anti-scatter slit, 6 mm of irradiated length of automatic mode and 0.04 rad of soller slit. XPS (PHI Versa-Probe II) with a scanning monochromated Al source (1100 eV survey scan; 50 W ; spot size, $200\text{ }\mu\text{m}$) was used to quantify the surface composition of the thin films. Surface morphology and interior structure of the MWNT-PANI thin films were investigated using a SEM (Helios Nanolab 600 Dual Beam Focused Ion Beam System) operating at 10.0 kV for medium and high resolution imaging. TEM observations of the synthesized MWNT-PANI nanocomposites were performed using a JEOL 2010TEM with an accelerating voltage of 200 kV . TEM samples were prepared by directly dropping the solutions onto carbon supported copper or nickel grids. The surface chemistry of the PANI-only and MWNT-PANI thin films were analyzed using a Raman Spectrometer (Kaiser Optical System) operating with a 785

nm laser for excitation to confirm the existence of MWNTs. Electrical conductivities were measured for films deposited on glass slides by using a standard four-point probe configuration (Jandel General Purpose System). A series of 4 or 5 measurements were taken on each film, and the measurements were averaged to give the final reported value with the standard deviation as an error range. The thickness of the PANI-based thin films was determined using a Veeco Dektak 150 profilometer. The surface area of the materials was measured by the BET technique, using an ASAP 2020 BET and monitoring nitrogen gas adsorption and desorption.

Electrochemical measurement of PANI-based thin films. A three-electrode cell was employed for the electrochemical measurements in the aqueous-cell test, where an Ag/AgCl electrode (BASi) (3 M NaCl) and a Pt wire were used as the reference and counter electrode, respectively. The PANI-only and MWNT-PANI thin films were used as the working electrodes. Cyclic voltammetry was performed between -0.2 and 0.8 V (vs. Ag/AgCl) at room temperature in 1.0 M H₂SO₄ solution using a potentiostat/galvanostat (Princeton Applied Research Model 263A). The weight of films deposited onto the substrate was measured by microbalance (Discovery microbalance in OHAUS).

Conclusions

In conclusion, we have demonstrated a facile phytic acid-mediated synthesis technique to prepare a highly porous 3D core (MWNT)-shell (PANI) conductive hydrogels with enhanced electrical conductivity and electrochemical activity. Phytic acid serves as (1) an excellent solvent for non-functionalized dispersions of pristine MWNTs in aqueous solution and (2) an excellent dopant/gelator to crosslink PANI NWs into hydrogels. The affinity of phytic acid to MWNTs enables the formation of well-dispersed MWNT-phytic acid complexes. The polymerization of PANI onto the surface of MWNTs enables the synthesis of MWNT-PANI composite hydrogels, and the as-fabricated nanostructured thin films form mesoporous networks with high surface area and directional pathways for efficient electron transport. The incorporation of MWNTs leads to improved electrical conductivity from 0.21 to 1.54 S cm⁻¹ as the loading of MWNTs increases to 5.0 wt.%. By improving the electrical conductivity, a maximal specific capacity of 609 F g⁻¹ is attained with 3.0 wt.% loading of MWNTs in the nanocomposite. Compared to the MWNT-PANI nanocomposites reported in the literature (see **Table S1**), the phytic acid-mediated hydrogel synthesis and assembly of NW-based electrodes not only demonstrate efficient electrochemical activities but open a low-cost route for electrode fabrication that can be translated to large-scale production for applications related to solar cells, pseudocapacitors, batteries, and sensors.

Acknowledgements

The authors wish to dedicate this paper to the memory of Officer Sean Collier, for his caring service to the MIT community and for his sacrifice.

Author contributions

P.-Y.C., A.M.B. and P.T.H. conceived the idea and designed the experiments. P.-Y.C. performed the synthesis, fabrication, characterization, and electrochemical testing. N.-M.D.C. performed TEM, XPS and porosity characterization. P.-Y.C., N.-M.D.C., M.N.H., A.M.B. and P.T.H. co-wrote the paper and all authors discussed the results and commented on the manuscript.

Funding sources

This work was supported by Eni, S.p.A (Italy) through the MIT Energy Initiative Program, by NSF for the Center for Chemical

Innovation under the NSF Center CHE-1305124, and by Institute for Collaborative Biotechnologies from the U.S. Army Research Office. P.-Y.C. and N.-M.D.C. acknowledge support from the MIT Energy Initiative Eni-MIT Energy Fellowship. M.N.H. is thankful for the support of a postdoctoral fellowship and N.-M.D.C. is thankful for a postgraduate scholarship both from the Natural Sciences and Engineering Research Council (NSERC) of Canada.

Supporting information

Top-down and cross-sectional SEM images of the PANI-only thin film, illustration of the large aggregation of MWNTs in the doctor-bladed MWNT-PANI thin film (loading of MWNTs ~10.0 wt.%), CV curves of the PANI-only and MWNT-PANI (loading of MWNTs ~3.0 wt.%) thin films at scan rates ranging from 1 mV s⁻¹ to 100 mV s⁻¹, summary of the electrochemical parameters from this work and the literature.

Notes and references

^aDepartment of Chemical Engineering, Massachusetts Institute of Technology, Cambridge, MA 02139 (USA)

^bThe David H. Koch Institute for Integrative Cancer Research, Massachusetts Institute of Technology, Cambridge, MA 02139 (USA)

^cDepartment of Materials Science and Engineering, Massachusetts Institute of Technology, Cambridge, MA 02139 (USA)

^dDepartment of Biological Engineering, Massachusetts Institute of Technology, Cambridge, MA 02139 (USA)

*Address correspondence to belcher@mit.edu and hammond@mit.edu

1. M. N. Hyder, N. J. Shah and P. T. Hammond, in *Multilayer Thin Films*, Wiley-VCH, Editon edn., 2012, pp. 393-435.
2. Y. Lu, W. He, T. Cao, H. Guo, Y. Zhang, Q. Li, Z. Shao, Y. Cui and X. Zhang, *Sci. Rep.*, 2014, 4.
3. L. Pan, G. Yu, D. Zhai, H. R. Lee, W. Zhao, N. Liu, H. Wang, B. C. K. Tee, Y. Shi, Y. Cui and Z. Bao, *Proc. Natl. Acad. Sci.*, 2012, 109, 9287-9292.
4. D. Zhai, B. Liu, Y. Shi, L. Pan, Y. Wang, W. Li, R. Zhang and G. Yu, *ACS Nano*, 2013, 7, 3540-3546.
5. Y. Zhao, B. Liu, L. Pan and G. Yu, *Energy Environ. Sci.*, 2013, 6, 2856-2870.
6. J.-W. Jeon, J. O'Neal, L. Shao and J. L. Lutkenhaus, *ACS Appl. Mater. Interfaces*, 2013, 5, 10127-10136.
7. H.-W. Park, T. Kim, J. Huh, M. Kang, J. E. Lee and H. Yoon, *ACS Nano*, 2012, 6, 7624-7633.
8. J. Tarver and Y.-L. Loo, *Thin Solid Films*, 2013, 539, 303-308.
9. K. Wang, J. Huang and Z. Wei, *J. Phys. Chem. C*, 2010, 114, 8062-8067.
10. P.-Y. Chen, M. N. Hyder, D. Mackanic, N.-M. D. Courchesne, J. Qi, M. T. Klug, A. M. Belcher and P. T. Hammond, *Adv. Mater.*, 2014, 26, 5101-5107.
11. J. Hur, K. Im, S. W. Kim, U. J. Kim, J. Lee, S. Hwang, J. Song, S. Kim, S. Hwang and N. Park, *J. Mater. Chem. A*, 2013, 1, 14460-14466.
12. N. A. Kumar, H.-J. Choi, Y. R. Shin, D. W. Chang, L. Dai and J.-B. Baek, *ACS Nano*, 2012, 6, 1715-1723.
13. M. N. Hyder, R. Kaviani, Z. Sultana, K. Saetia, P.-Y. Chen, S. W. Lee, Y. Shao-Horn and P. T. Hammond, *Chem. Mater.*, 2014, 26, 5310-5318.
14. M. N. Hyder, S. W. Lee, F. Cebeci, D. J. Schmidt, Y. Shao-Horn and P. T. Hammond, *ACS Nano*, 2011, 5, 8552-8561.
15. C.-M. Chang, C.-J. Weng, C.-M. Chien, T.-L. Chuang, T.-Y. Lee, J.-M. Yeh and Y. Wei, *J. Mater. Chem. A*, 2013, 1, 14719-14728.
16. S. R. Sivakkumar, W. J. Kim, J.-A. Choi, D. R. MacFarlane, M. Forsyth and D.-W. Kim, *J. Power Sources*, 2007, 171, 1062-1068.

17. H. Wei, H. Gu, J. Guo, S. Wei and Z. Guo, *J. Electrochem. Soc.*, 2013, 160, G3038-G3045.
18. H. Zhang, G. Cao, W. Wang, K. Yuan, B. Xu, W. Zhang, J. Cheng and Y. Yang, *Electrochim. Acta*, 2009, 54, 1153-1159.
19. G. Otkhrov, D. Pankratov, G. Shumakovich, M. Khlupova, Y. Zeifman, I. Vasil'eva, O. Morozova and A. Yaropolov, *Electrochim. Acta*, 2014, 123, 151-157.
20. S. Jo, H. Jeong, S. R. Bae and S. Jeon, *Microchem. J.*, 2008, 88, 1-6.
21. G. Xiaoyu, M. Yun, Y. Pingping, W. Ying and Y. Haifeng, *Mater. Res. Express*, 2014, 1, 025403.
22. J.-C. Chiang and A. G. MacDiarmid, *Synt. Met.*, 1986, 13, 193-205.
23. I. Sapurina and J. Stejskal, *Polym. Int.*, 2008, 57, 1295-1325.
24. P. Paik, R. Manda, C. Amgoth and K. Santhosh Kumar, *RSC Adv.*, 2014, 4, 12342-12352.
25. J.-W. Jeon, R. Sharma, P. Meduri, B. W. Arey, H. T. Schaefer, J. L. Lutkenhaus, J. P. Lemmon, P. K. Thallapally, M. I. Nandasiri, B. P. McGrail and S. K. Nune, *ACS Appl. Mater. Interfaces*, 2014, 6, 7214-7222.
26. J. Yan, T. Wei, Z. Fan, W. Qian, M. Zhang, X. Shen and F. Wei, *J. Power Sources*, 2010, 195, 3041-3045.

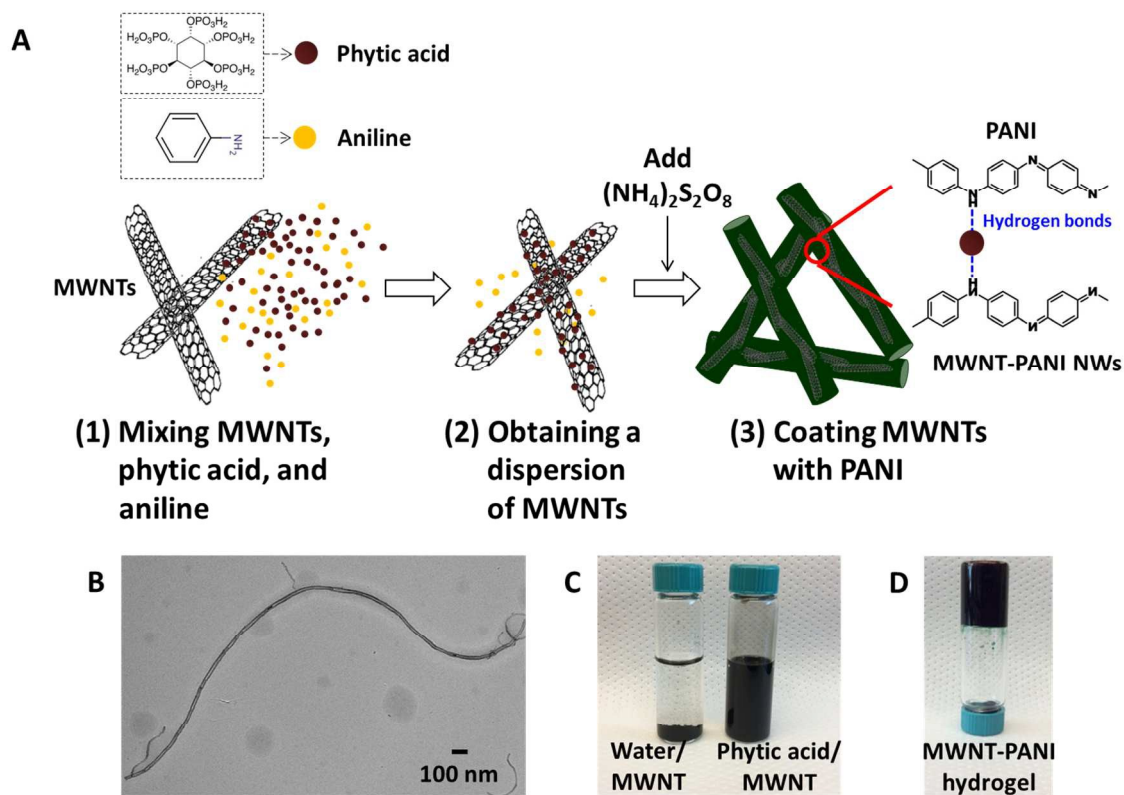


Figure 1. MWNT-PANI hydrogels are assembled via polymerizing PANI in a dispersion of MWNTs in phytic acid. A. Schematic illustration of the process to fabricate MWNT-PANI conductive hydrogels, including (1) mixing MWNTs, phytic acid, and aniline, (2) obtaining a dispersion of MWNTs, and (3) coating MWNTs with PANI. B. TEM image of one string of pristine MWNT (diameter ~15 nm). C. Illustration of the aggregation of MWNTs in water, and their dispersion in a phytic acid solvent. D. As-polymerized MWNT-PANI conductive hydrogel.

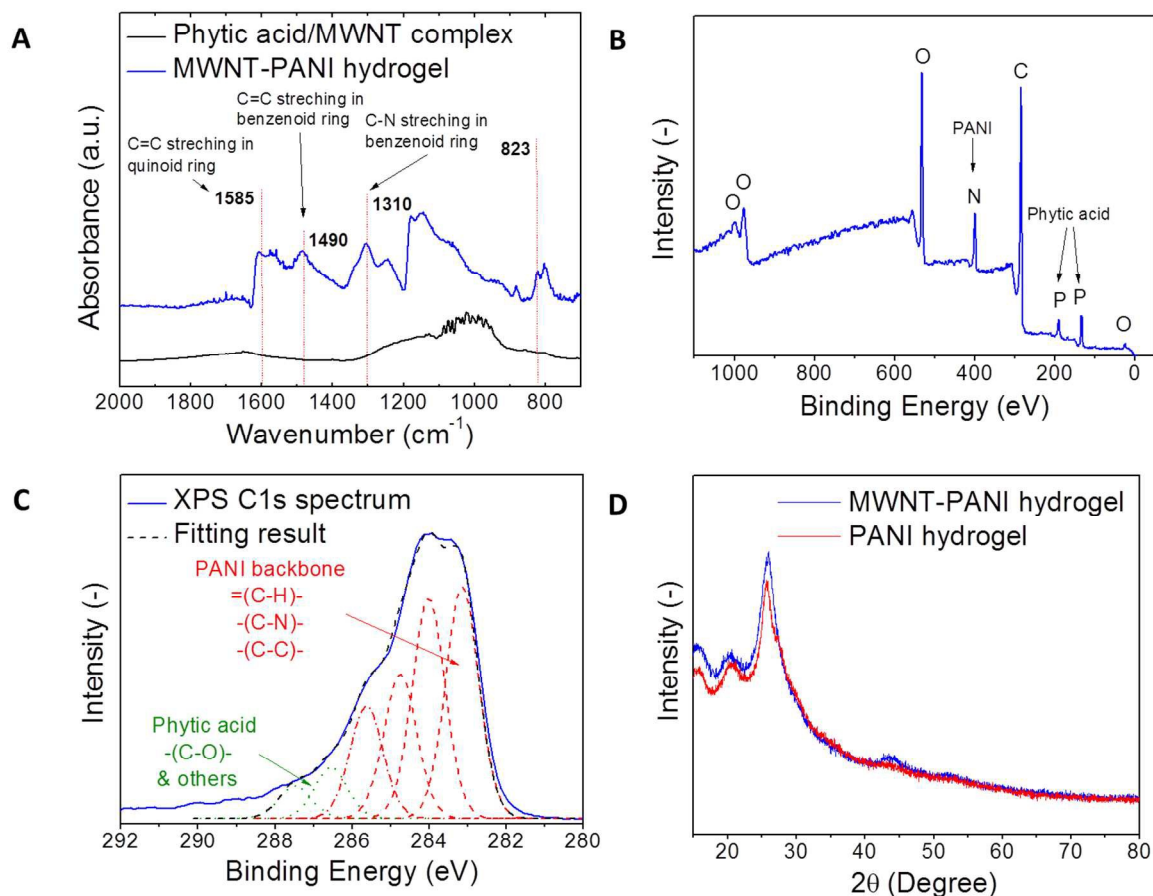


Figure 2. A. FTIR spectra of the phytic acid/MWNT complex and MWNT-PANI hydrogel. The peaks at 1310 cm^{-1} , 1490 cm^{-1} and 1585 cm^{-1} are attributed to C-N stretching, C=C stretching in the benzenoid ring, and C=C stretching in the quinoid ring, respectively. The observation of these peaks indicates the formation of PANI in the hydrogel. B. XPS survey scan of the MWNT-PANI thin film. The N and P peaks indicate the presence of PANI in the emeraldine state doped by phytic acid. C. XPS C1s spectrum and deconvolution of peaks for the MWNT-PANI thin film. The C-N, C-C, and =CH- moieties at lower binding energies originated from the backbone of PANI; carbon-oxygen groups and other carbon chemistries at higher binding energies belong to the phytic acid. D. XRD analysis of the PANI-only and MWNT-PANI hydrogels, indicating that the addition of MWNTs into PANI hydrogels does not affect the crystallinity of PANI coating.

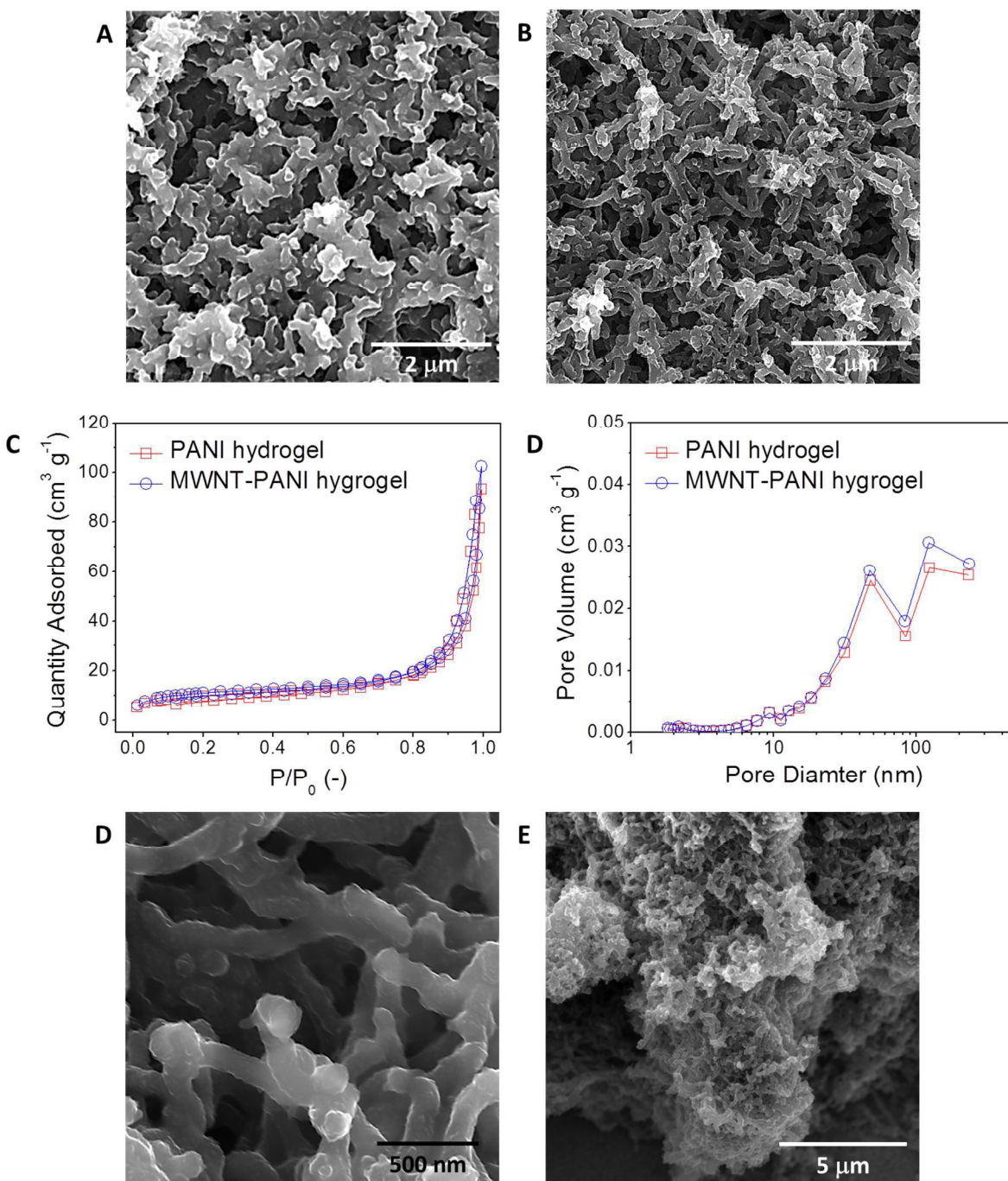


Figure 3. A. Top-down SEM image of a PANI-only thin film. B. Top-down SEM image of a MWNT-PANI thin film. MWNT-PANI hydrogels exhibit continuous interconnected NW-like features and a high porosity. B. BET nitrogen adsorption and desorption isotherms used to calculate the surface area, and C. BJH pore size distribution for PANI-only and MWNT-PANI thin films. D. High resolution top-down SEM image of a MWNT-PANI thin film. E. Cross-sectional SEM image of a MWNT-PANI thin film.

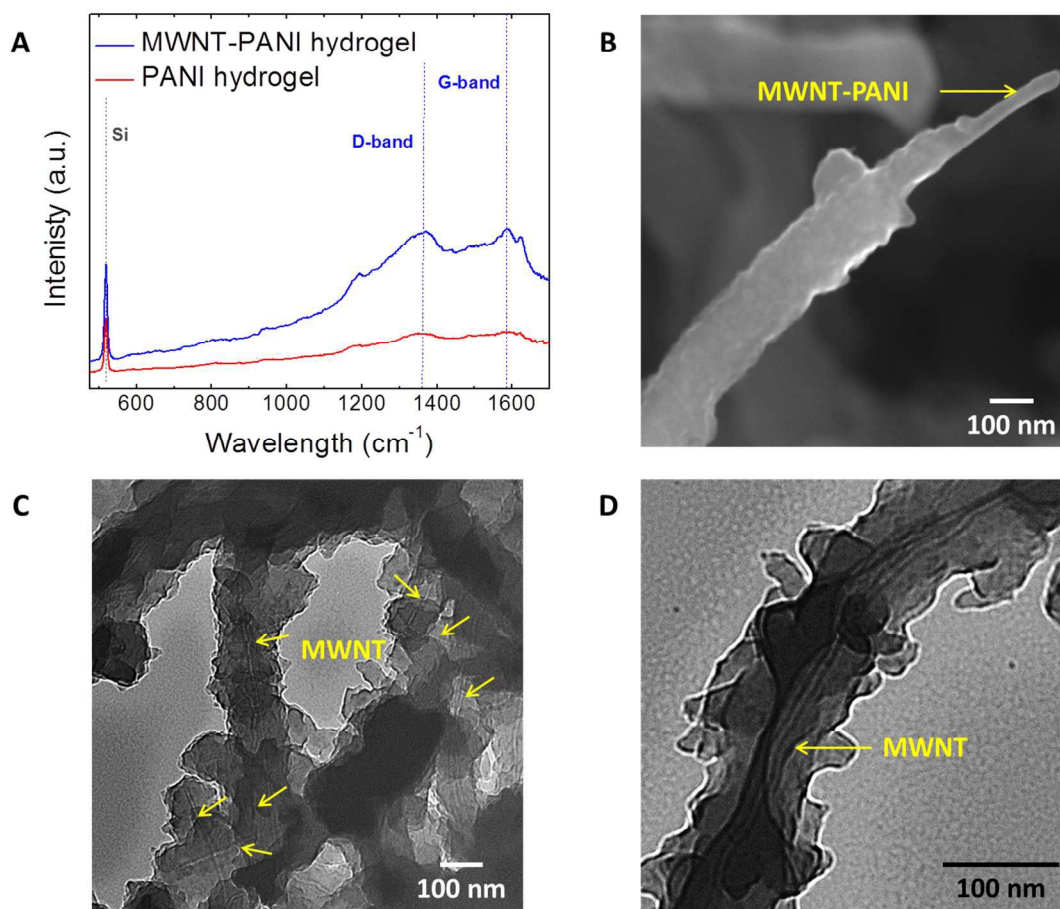


Figure 4. The polymerization of PANI in the dispersion of MWNT in phytic acid results in the formation of a MWNT-PANI core-shell structure. A. Raman spectra comparing the PANI-only and MWNT-PANI hydrogels. B. High resolution SEM image of MWNT-PANI core-shell nanostructure. C and D. TEM images of the MWNT-PANI complexes. The MWNTs are visible as well-dispersed elements within the PANI NWS.

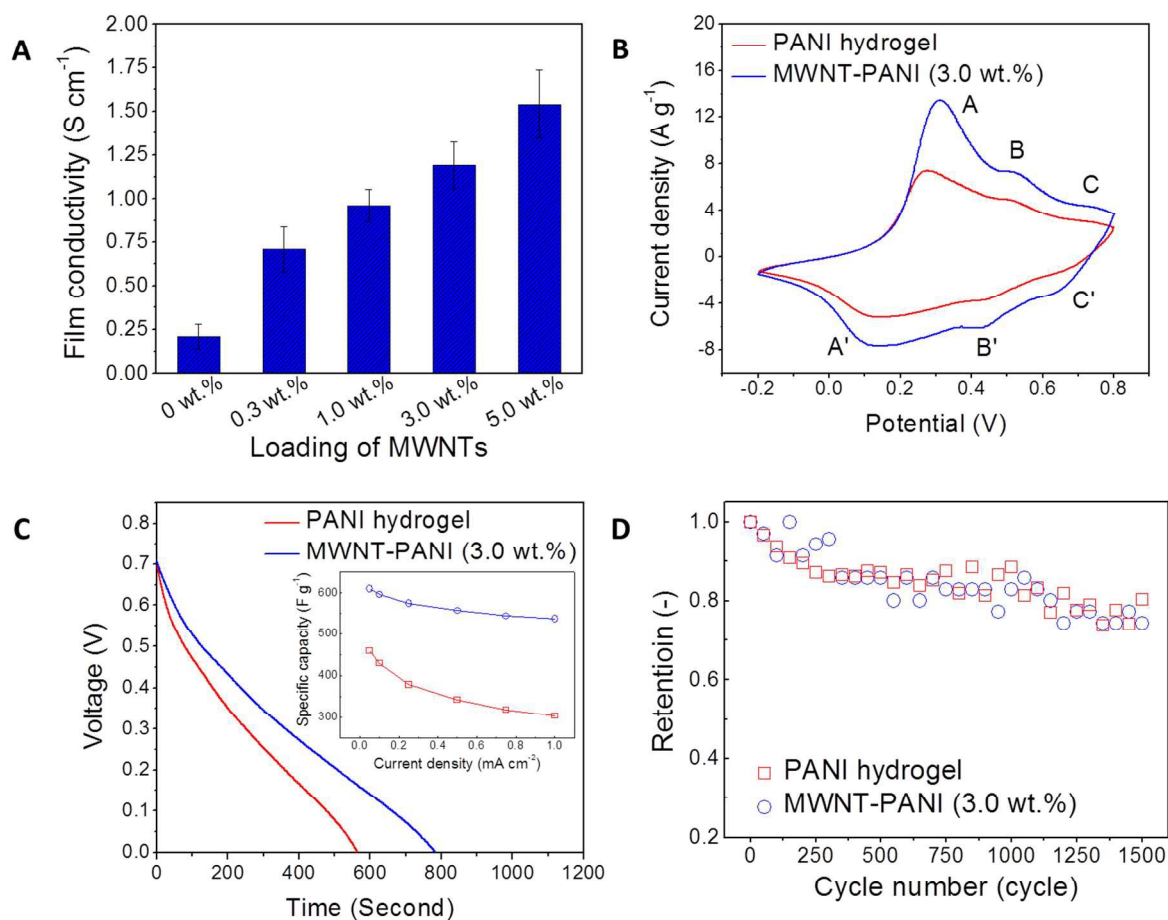


Figure 5. Incorporating MWNTs within PANI thin films significantly improves their conductivity and specific capacitance. A. Electrical conductivity measurements on the PANI and MWNT-PANI thin films. B. CV curves of the PANI and MWNT-PANI (with the loading of MWNTs ~ 3.0 wt.%) thin films at a scan rate of 10 mV s^{-1} . C. Galvanostatic charge-discharge curves for the PANI and MWNT-PANI (with the loading of MWNTs ~ 3.0 wt.%) thin films, with an inset showing their specific capacitances as a function of charge-discharge current densities. D. Cycling stability of PANI and MWNT-PANI (with the loading of MWNTs ~ 3.0 wt.%) thin films under a charge-discharge current of 3 mA cm^{-2} .